# Research On Hardware Design of In-Wheel Motor Drive Controller for New Energy Vehicles Based on STM32 Microcontroller

Yiqing Zhu\*

College of Automation, Nanjing University of Posts and Telecommunications, Nanjing, China

\* Corresponding Author Email: 2794819685@gg.com

**Abstract.** Against the backdrop of the promotion of the national "dual carbon" policy and the upgrading of environmental protection requirements, new energy vehicles (NEVs) have become the preferred means of transportation for an increasing number of consumers. This paper designs a hardware circuit for the in-wheel motor (IWM) drive controller based on the STM32F103 series microcontroller, with a focus on optimizing the power drive and conversion circuit centered around insulated gate bipolar transistor (IGBT), the optocoupler isolation circuit, the voltage and current sampling circuit, etc. The feasibility of the control strategy adapted to the hardware is verified through MATLAB/Simulink platform. The results show that this control strategy can achieve stable control of the IWM. This research provides a feasible technical reference for the hardware design and optimization of the IWM drive system of NEVs.

Keywords: New energy vehicles; In - wheel motor; Hardware circuit; Simulation.

## 1. Introduction

Driven by the global energy transition and environmental demands, NEVs have emerged as a central direction for the automotive industry. With robust policy support, China has witnessed a continuous expansion of its NEV market. In 2024, national NEV sales reached 12.866 million units, accounting for 40.9% [1] of total automobile sales. From January to July 2025, sales further climbed to 8.22 million units, representing 45.0% of the market and marking a 38.5% [2] year-on-year increase. These figures underscore the growing market penetration of NEVs.

The drive control system constitutes a foundational component of NEV technology, with its performance being a critical determinant of vehicular dynamics and efficiency. Drive control technology is mainly divided into centralized control and distributed control. Centralized control is defined by the use of a solitary controller for holistic powertrain administration, offering benefits of simplified logic and elevated integration. The distributed control, however, adopts a multi-controller cooperative working mode. By distributing control functions to various execution units, it possesses significant advantages including fast response speed, strong fault tolerance, and high expansion flexibility. It is particularly suitable for multi-power source cooperative control scenarios, enabling a more precise match to dynamic demands under complex working conditions [3].

As an innovative form of drive, the IWM lends itself naturally to distributed control architectures due to the elimination of traditional transmission components, the subsequent improvements in transmission efficiency and flexibility of layout. Its independent driving capability enables direct and precise coordinated control of individual wheels, making IWM technology a key research direction for implementing distributed control in NEV drive systems. Among IWM technologies, the permanent magnet synchronous motor (PMSM) holds significant application value in the NEV drive field, owing to its compact structure, high power density, and excellent torque characteristics [4]. To meet the high-efficiency control demands of IWMs, this paper designs and develops a hardware system for a PMSM-based IWM drive controller using an STM32-series microcontroller. The control strategy this paper chosen is modeled and tested by MATLAB/Simulink platform.

## 2. Overview of IWM

The IWM is a novel type of power unit that integrates the motor directly into the wheel hub. It eliminates traditional transmission components such as the clutch, reducer, drive shaft, and differential, thereby enhancing the overall spatial utilization of the vehicle [5]. It offers advantages including rapid response and the capability for independent four-wheel drive and control. These features contribute to improved vehicle dynamic performance and handling flexibility, providing a new direction for the development of vehicle electrification.

#### 2.1. Structure and Classification of IWM

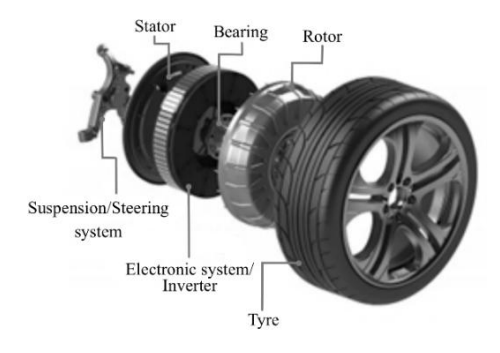
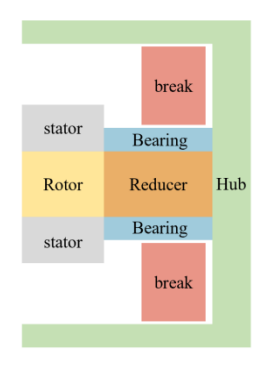
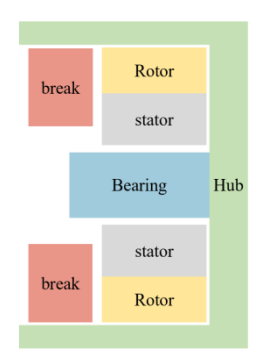


Fig. 1 The structure of IWM

As an integrated drive unit, the IWM typically consists of essential components including a stator, rotor, bearings, a housing, and windings. It is also associated with the suspension/steering system and inverter. The specific configuration is illustrated in Fig. 1. Its working principle can be summarized as follows: during vehicle operation, the inverter first converts the direct current from the onboard power battery into alternating current, which is then supplied to the motor windings. Once energized, the windings generate an alternating magnetic field. This field interacts electromagnetically with the permanent magnets on the rotor, causing the rotor to rotate around the stator. Since the rotor is directly connected to the wheel hub, it ultimately drives the wheel, thereby converting electrical energy into the mechanical energy required for vehicle propulsion.





(a)Geared inner-rotor

(b)Direct-drive outer-rotor

Fig. 2 Schematic diagram for comparison of the two structures

Based on the drive configuration, IWMs can be categorized into two types: direct-drive with an outer-rotor structure, and geared-drive with an inner-rotor structure, as illustrated in Fig. 2.

The geared-drive IWM utilizes a high-speed inner-rotor motor. A fixed-ratio reduction reducer is installed between the motor and the wheel to regulate speed and boost torque. In contrast, the direct-drive IWM employs a low-speed outer-rotor motor. The motor's outer rotor is directly affixed to the wheel rim, eliminating the need for a reducer. Consequently, the motor speed is identical to the wheel speed [6]. A comparison of the advantages and disadvantages of these two drive configurations is presented in Table 1.

Geared Inner-Rotor Item Direct-Drive Outer-Rotor Outer rotor connected to the rim, Structural Inner rotor, outer stator, equipped stator fixed to the axle, without a with a reducer. feature reducer. Simple structure, high efficiency, fast High power density, compact & Advantages lightweight, high output torque. response, low noise & vibration Adds space/weight, efficiency loss, Requires high current for high torque, Disadvantages prone to wear, difficult maintenance narrow high-efficiency range Commercial vehicles, engineering **Typical** Passenger vehicles, electric bicycles application machinery

Table 1. Characteristics of direct-drive and geared IWM

## 2.2. Current Status of IWM Applications

Currently, the large-scale commercial application of IWM has not yet been realized, with their usage primarily confined to specific areas. Within the realm of special-purpose vehicles, IWMs are utilized in off-road utility vehicles and port transfer carts, leveraging their advantages of a compact structure and flexible layout to meet operational demands in complex terrains and confined spaces. In low-speed, short-range scenarios, certain micro electric vehicles and logistics distribution vehicles have initiated small-scale trials. The high energy efficiency and minimal space occupancy of IWMs align well with the requirements of these applications. In the NEV area, several manufacturers are exploring the potential of four-wheel independent drive by incorporating IWM technology. Models such as Voyah Zhuiguang and Dongfeng E70 have demonstrated enhanced cornering stability and braking performance through precise torque control at each wheel, thereby accumulating valuable practical data for technological iteration. Furthermore, the technology is being trialed in various concept cars.

Although the IWM is widely regarded as the ultimate form of future distributed drive systems due to its numerous prominent advantages, its application in new EVs still faces several technical challenges, which are primarily manifested in the following aspects. First, the increase in unsprung mass raises the load on the suspension system, adversely affecting ride comfort and handling stability, while also accelerating tire wear. Second, thermal demagnetization is a critical issue, where confined space and weight limits restrict heat dissipation, potentially causing permanent magnet demagnetization and motor performance loss. Third, vehicle integration becomes more complex. The distributed drive architecture alters power transmission and force distribution, yet design standards and testing protocols remain underdeveloped, creating high barriers to industrialization. Additionally, factors such as high manufacturing costs, difficult maintenance, and unproven reliability under complex road conditions further hinder large-scale adoption. Addressing these issues requires concerted efforts in technological breakthroughs and industrial collaboration [7, 8].

# 3. Hardware Circuit Design

## 3.1. Overall System Architecture

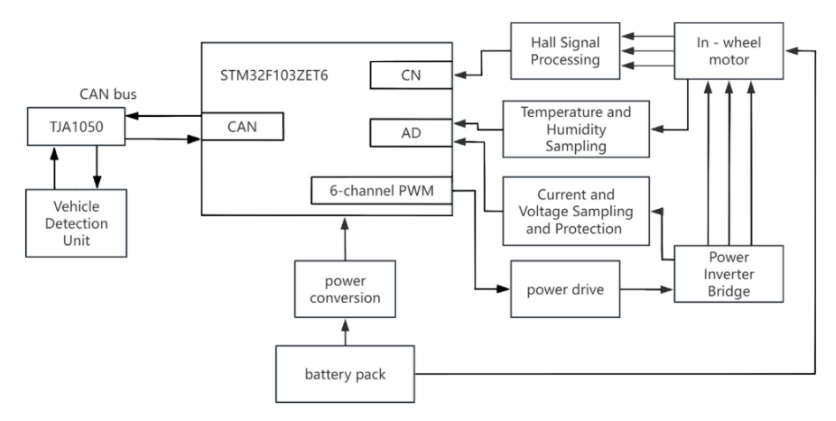


Fig. 3 Block diagram of the motor control system hardware

The system employs an STM32F103ZET6 microcontroller as the core controller, which operates in coordination with external nodes, such as the vehicle detection unit, and various functional modules related to the IWMs, forming a distributed control architecture. The vehicle adopts a rear-wheel drive configuration, with a pair of IWMs responsible for propulsion. The core controller acquires global vehicle status signals from the vehicle detection unit via the CAN bus. Simultaneously, it uses its integrated functions, including Hall signal processing, current and voltage sampling, temperature and humidity monitoring, and over-current and over-voltage protection, to obtain critical IWM parameters such as rotor position, operating current and voltage, and ambient temperature and humidity. Based on a torque distribution algorithm, it generates control commands. The microcontroller outputs six channels of Pulse Width Modulation (PWM) signals according to the algorithm. These signals are amplified by the power driver module to drive the power inverter bridge, thereby achieving precise control of the IWMs. The operating power for both the microcontroller and the peripheral circuits is supplied by the vehicle battery, which is conditioned to appropriate voltage levels by a power conversion module.

## 3.2. Master Chip

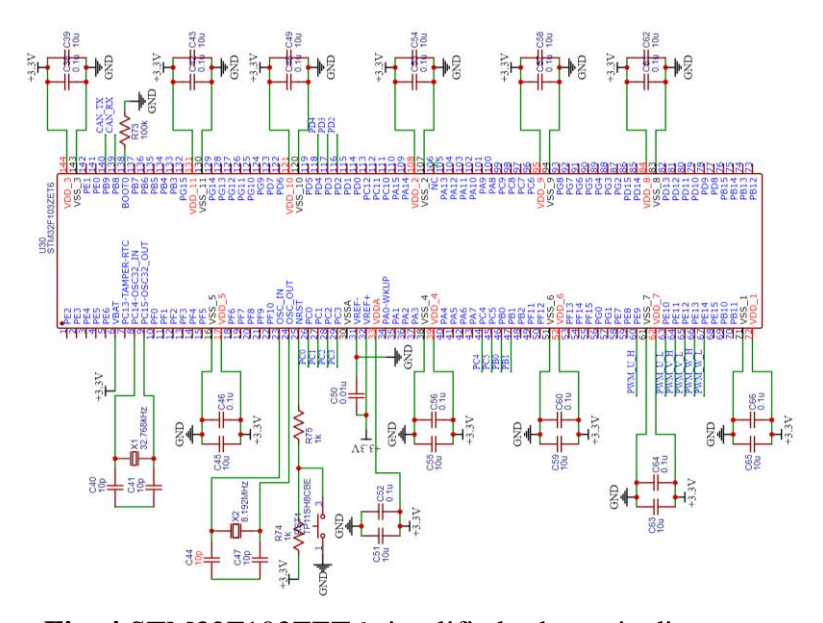


Fig. 4 STM32F103ZET6 simplified schematic diagram

In this system, STM32F103ZET6 is selected as the main controller, which undertakes the core tasks of signal acquisition, logic operation, drive control and communication interaction. Its performance and resource configuration directly affect the system stability and control accuracy.

The chip is based on the ARM Cortex-M3 core and operates at a maximum frequency of 72 MHz. It supports single-cycle multiplication and hardware division, enabling it to efficiently process real-time tasks such as three-phase inverter PWM waveform generation, high-frequency sampling of Hall sensor signals, and CAN communication, ensuring all operations are completed within their timing constraints. In terms of peripherals, it integrates one CAN controller (supporting the CAN 2.0A/B protocol) that can be used with a TJA1050 transceiver to build a high-reliability communication network. It is equipped with eight 16-bit timers, allowing it to produce complementary PWM output with dead-time control for directly driving a three-phase full-bridge inverter circuit. It incorporates three 12-bit ADC modules, which support DMA control and timer synchronization triggering for acquiring analog signals from multiple sensors. Regarding memory resources, it includes 512 KB of Flash memory and 64 KB of SRAM, meeting the requirements for running complex algorithms. Its operating voltage range is 2.0 V to 3.6 V, and its operating temperature range is -40 °C to 85 °C, making it suitable for industrial environments. Additionally, the mature development environment and extensive open-source libraries available help reduce development difficulty and accelerate project progress.

**Table 1**. Three Scheme comparing

Numble	Scheme 1	Scheme 2	Scheme 3
1	456	456	123
2	789	213	644
3	213	654	649

#### 3.3. Peripheral Circuit

The peripheral circuitry is designed around the core motor control functions, encompassing the power supply circuit, power drive and conversion circuit, position detection circuit, current/voltage Sampling circuit, current/voltage protection circuit, and the CAN bus communication circuit. These modules work in concert to achieve power supply, driving, status monitoring, safety protection, and data communication.

#### 3.3.1 Power circuit

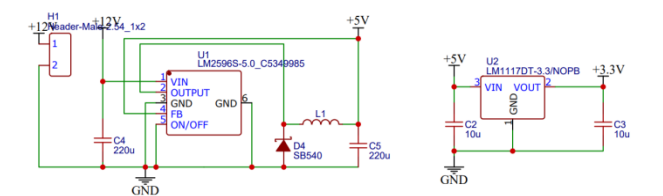


Fig. 5 Power circui

The power for both the microcontroller and its peripheral circuits is supplied by the vehicle's 12 V low-voltage system. This 12 V input is first stepped down to 5 V via an LM2596 converter, and then further regulated to 3.3 V by an LM1117 regulator. The LM2596 chip is suitable for conversions with a significant voltage differential, owing to its 3 A output current capability and wide input voltage range of 0.3 V to 45 V, which ensures stable operation from the 12 V source. In contrast, the circuit configuration of the LM1117 is more compact, requiring only filter capacitors to achieve the 5 V to 3.3 V conversion. It offers higher accuracy and demonstrates distinct advantages for applications with smaller voltage differentials.

#### 3.3.2 Power drive and conversion circuit

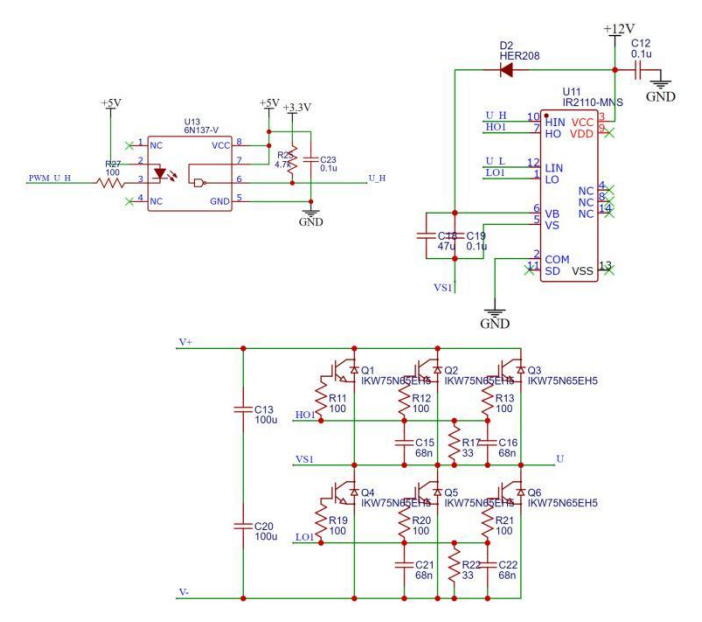


Fig. 6 Power drive and power conversion circuit

The six PWM signals input to the power drive circuit are first isolated by the optocoupler circuit located in the upper-left section of Fig. 6. The drive chip selected is the IR2110-MNS, which amplifies the PWM signals to a 12 V level before supplying them to the power conversion circuit.

As shown in Fig. 6, each phase of the power inverter consists of three IKW75N65EH5 IGBTs connected in parallel, which form the upper and lower bridge arms respectively. Peak Gate Driving Current of a Single IGBT

$$I = Q_g / T, \tag{1}$$

Where T denotes the turn-on/turn-off time, and Q<sub>g</sub> denotes the total gate charge. Taking

 $Q_g = 120\,$  nC and  $T = 0.2\,$  µs,  $I = 0.6\,$  A. Since each bridge arm phase employs a set of three paralleled IGBT, the total required peak drive current for a single set is 1.8 A. IR2110-MNS features a minimum peak drive current of 3 A and a typical value of 4 A, which adequately satisfies the driving requirements of the IGBTs [9].

#### 3.3.3 Position detection circuit

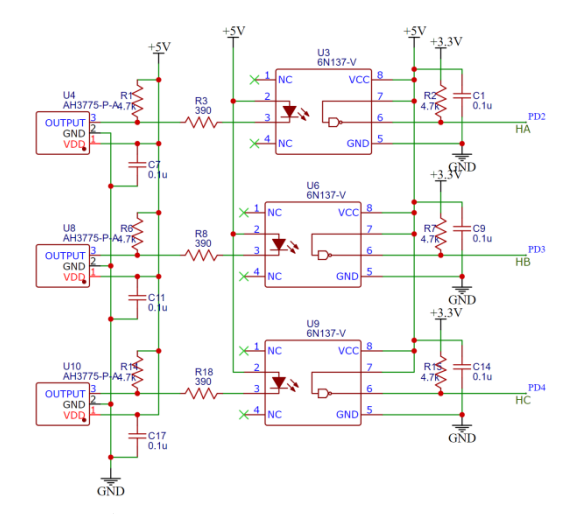


Fig. 7 Position detection circuit

The position detection circuit utilizes the Hall effect latch AH3775-P-A, which provides a digital output. Three such latches are mounted on the stator of the IWM with a 120-degree electrical angle spacing, supplying the system with three-phase position detection signals (HA, HB, HC). The high

and low level combinations of these three signals are used to delineate corresponding sectors. A greater number of motor pole pairs results in a higher quantity of sectors within the same mechanical angle, thereby enhancing the resolution and accuracy of the position detection.

#### 3.3.4 Voltage / current sampling circuit

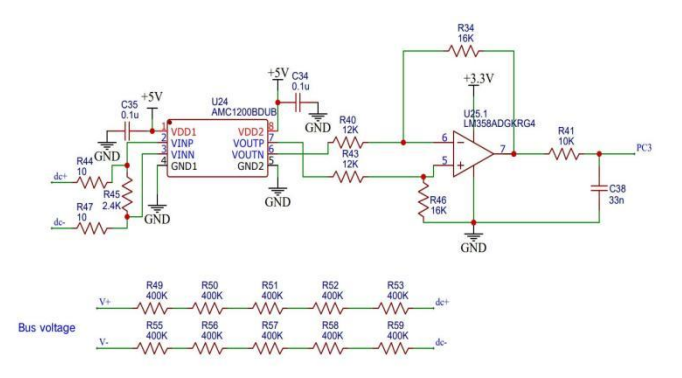


Fig. 8 Voltage sampling circuit

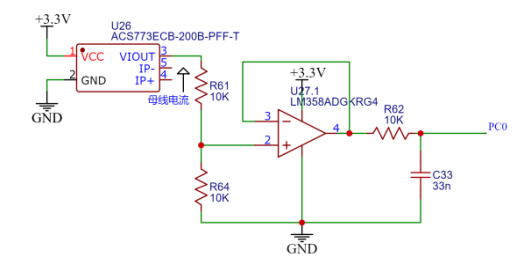


Fig. 9 Current sampling circuit

Both the voltage and current sampling circuits employ Hall-effect sensors, which provide inherent electrical isolation and eliminate the need for additional isolation circuitry. Fig. 9 shows the circuit diagram for bus current detection. For three-phase AC current detection, the filter circuit must be omitted.

The voltage sampling circuit first performs voltage division on the input high voltage, takes the voltage across resistor R45 and sends it to the sensor. After conversion by the sensor, the signal is processed by a differential amplifier circuit and a filter circuit in sequence, and finally input to the microcontroller. The voltage division stage reduces the input voltage to 0.0006 times its original value. After being amplified 8 times by the sensor (the fixed gain of the sensor is 8) and then 1.33 times by the differential amplifier circuit, the final output voltage is approximately 0.0064 times the input voltage.

For current sampling, the output signal of the sensor is divided using two resistors, then undergoes voltage following via a non-inverting proportional amplifier circuit, and finally is input to the microcontroller after passing through a filter circuit. This Hall current sensor outputs a reference voltage of 1.65 V when there is zero current input. Its output voltage can be calculated using the sensitivity parameter of 6.6 mV/A. Given that the voltage division ratio of the voltage divider circuit is 0.5, the relationship between the input voltage and input current is as follows:

$$U = (2.5 V + 0.0066 I) / 2.$$
 (2)

#### 3.3.5 Current/voltage protection circuit

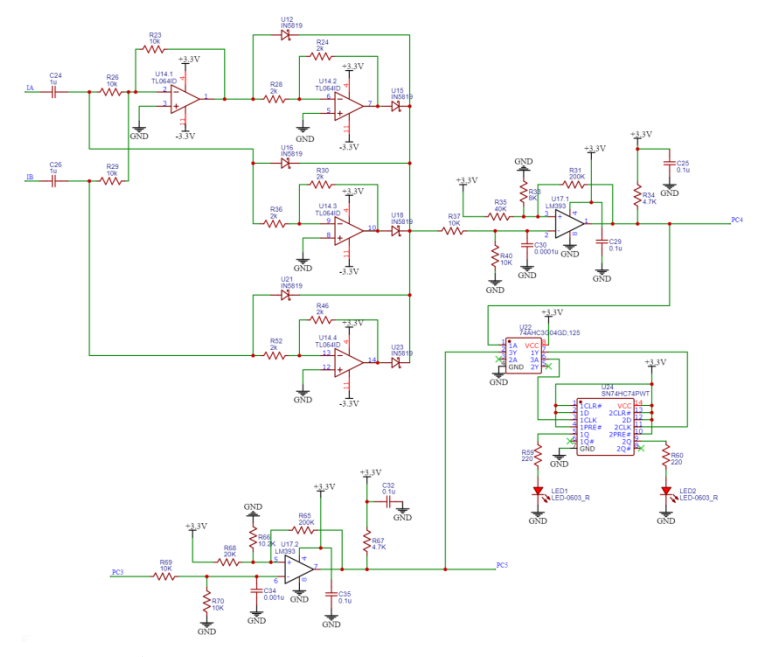


Fig. 10 Current/voltage protection circuit

The protection circuit is critical for preventing damage to the power modules and the motor stator windings caused by overcurrent. The upper section of Fig. 10 illustrates the three-phase AC protection circuit. Since the sum of the three-phase currents

$$IA + IB + IC = 0, (3)$$

it is sufficient to sample only two of the phase currents to achieve effective three-phase protection. The input to this circuit is derived from the Hall current sensors. The selected sensors' outputs include a DC bias of VCC / 2, which is first removed by a coupling capacitor to block the DC component and pass only the AC signal.

voltage and overcurrent protection circuits is a comparator circuit. A protection threshold is set at the non-inverting input of the comparator by adjusting resistor values, while the signal under test is fed into the inverting input. When the test signal exceeds this threshold, the comparator output switches from a high to a low logic level. The microcontroller, upon detecting this falling edge, immediately initiates protective actions [10]. The lower-right section of Fig. 10 depicts the alarm indicator circuit. When the comparator output goes low, the Q output of the D flip-flop is set high, causing the alarm indicator light to illuminate steadily.

#### 3.3.6 CAN bus communication circuit

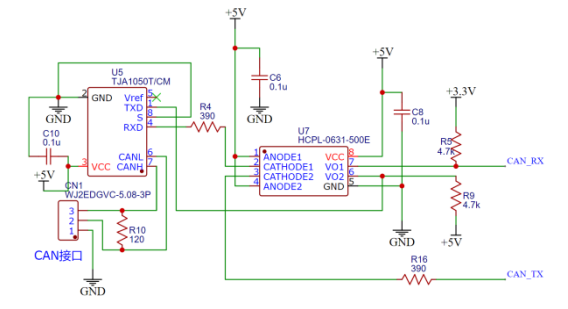


Fig. 11 CAN bus communication circuit

The CAN bus facilitates data exchange between the vehicle controller and the microcontroller. Through this bus, the microcontroller receives commands from the vehicle controller and publishes the motor's operational status parameters to the CAN network, making them available for acquisition by other nodes [9]. The circuit is presented in Fig. 11.

The isolation chip adopted in this circuit is HCPL-0631. The selection reason is that, as an integrated dual-channel optocoupler, it features enhanced common-mode rejection compared to two discrete optocouplers. Its integrated package strengthens immunity against common-mode noise on the bus, thereby ensuring the timing consistency of transceiver signals during high-speed CAN communication.

#### 3.3.7 Sensor circuit

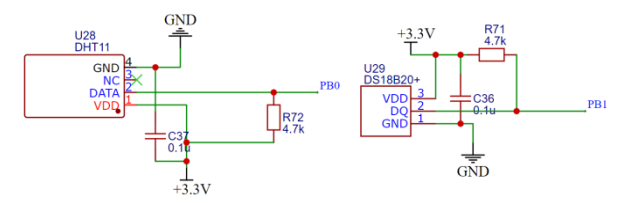


Fig. 12 Sensors circuit

The DHT11 humidity sensor is selected for its robust digital signal transmission, which provides strong resistance to interference and makes it well-suited for the complex electromagnetic environment of the motor compartment. For temperature sensing, the DS18B20 is chosen because it supports multi-point serial monitoring, allowing for flexible deployment across different parts of the motor to facilitate temperature acquisition from multiple zones. Both sensors are digital types, eliminating the need for analog-to-digital conversion and thereby simplifying the circuit design. The two circuits are shown in Fig. 12.

#### 2.3.8 Pin assignment

To meet the hardware functional requirements of the IWM controller, the pin assignment outlined in Table 2.1 was completed based on the specific function of each pin. This configuration utilizes a total of 19 pins from the PE, PB, PC, and PD series, enabling the functional adaptation and integration of all hardware interfaces.

6-channel PWM waves	PE9 PE10 PE11 PE12 PE13 PE14
CAN communication transceiver	PB8 PB9
Current sampling (bus current, three-phase AC IA, IB)	PC0 PC1 PC2
Voltage sampling	PC3
Humidity / temperature sensor	PB0 PB1
Current / voltage protection	PC4 PC5
Position detection	PD2 PD3 PD4

**Table 2**. Pin assignment table

## 4. Simulation

Simulink, a module-based visual simulation environment within MATLAB, is designed for multi-domain simulation and model-based design. It supports system design, simulation, automatic code generation, along with continuous testing and verification of embedded systems. Based on these functional capabilities, this study employs this tool to construct a simulation model for the Field-Oriented Control (FOC) strategy.

## 4.1. Control Strategy

The FOC strategy adopted in this simulation model is based on coordinate transformation theory. It decomposes the motor's stator current into two orthogonal components: the excitation component and the torque component. This enables decoupled control of flux and torque, thereby imparting the AC IWM with control characteristics analogous to those of a DC motor [11]. Although FOC involves relatively high computational complexity, it offers fast dynamic response, stable low-speed performance, and high technological maturity, leading to its widespread application in the field of

IWM control. In this system, the microcontroller acts as the central controller. Signals such as speed and current, collected by sensors, are processed by PI regulators in the speed loop and current loop. Subsequently, the space vector pulse width modulation (SVPWM) algorithm generates PWM waves with varying duty cycles to alter the motor's operating state, forming a closed-loop feedback system that ensures stable motor operation.

#### 4.2. Simulation Model

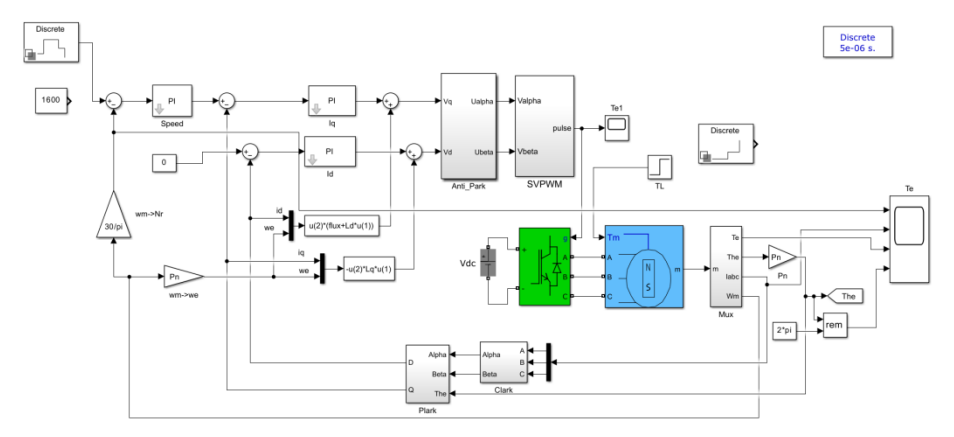


Fig. 13 System simulation model

A simulation model, as illustrated in Fig. 13, was constructed in Simulink. It incorporates the following core modules: Clarke/Park transformation and inverse transformation modules, PI controller modules, an SVPWM module, an IWM plant model, an inverter model, and measurement feedback modules that emulate the functionality of hardware sensors [12]. The given speed and load torque inputs can be replaced with step functions to test the system's dynamic response.

## 4.3. Simulation Results

The parameters of the PMSM employed in the simulation are listed in Table 3.

Table 3. PMSM parameters

Stator phase resistance $\Omega$	0.05	Flux linkage /V·s	0.06
D-axis Inductance /mH	1.5	Inertia /kg·m <sup>2</sup>	0.5
Q-axis Inductance /mH	1.5	Pole pairs	10

Before the simulation, the target speed and load torque were set. The input speed step function is shown in Fig 14. A load torque of 20 Nm was applied at 7.5 s. The simulation result is shown in Fig. 15.

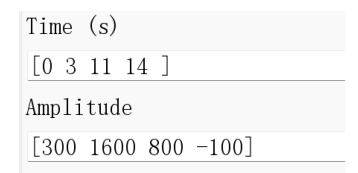


Fig. 14 Step parameters

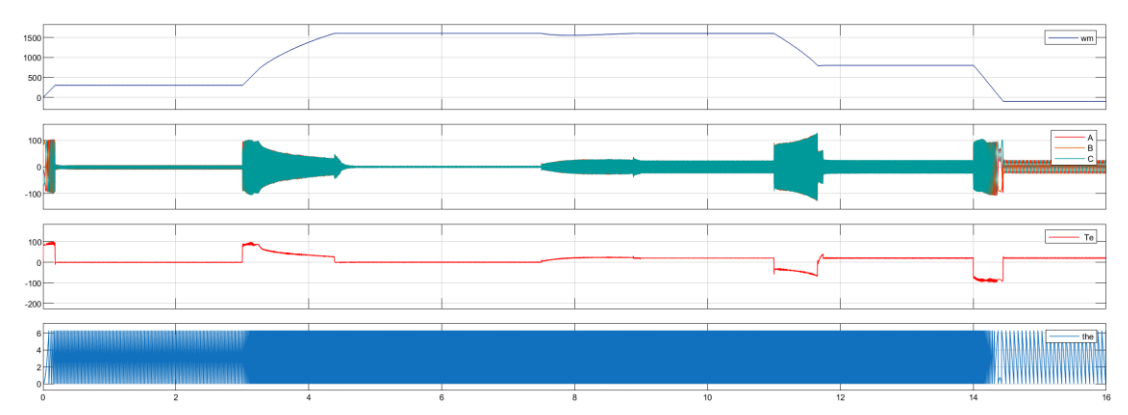


Fig. 15 Simulation result

The speed waveform demonstrates a rapid tracking response to the reference speed, achieving a steady state at 1600r/min. After a 20 Nm load torque is applied at this speed, the system rapidly recovers and stabilizes following a dynamic adjustment process. Although the electromagnetic torque exhibits brief fluctuations during acceleration and load changes, it quickly converges to a stable value. The overall control performance is effective.

As can be observed from Fig. 16, the three-phase AC currents of the PMSM exhibit a sinusoidal waveform. This aligns well with the theoretical expectation, showing a high degree of sinusoidality and few harmonics.

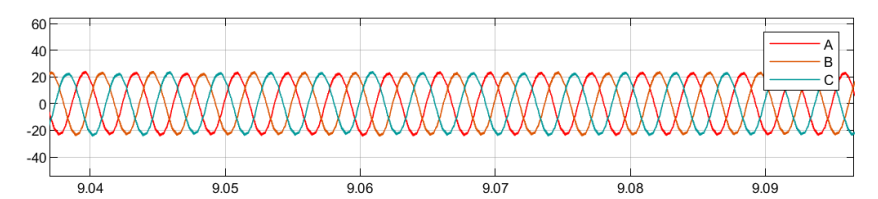


Fig. 16 Enlarged waveforms of three-phase AC

# 5. Summary

- 1) This paper presents the design of a hardware circuit for an IWM controller based on the STM32F103ZET6 microcontroller. The design integrates functional modules including power supply, power drive, sensing, communication, and protection, thereby achieving power delivery, motor driving, data exchange, and safety protection. It provides a reliable hardware foundation for the application of IWM technology in NEVs.
- 2) Simulink simulation results demonstrate the effectiveness of the proposed FOC control strategy and the rationality of the parameter configuration. The motor achieves a high rotational speed under a specified load torque, indicating satisfactory control performance.

## References

- [1] Zheng, X. Q. Domestic new energy vehicle sales increased by 27.4% in July 2025. Automobile Review, 2025, (09): 110-111.
- [2] Zheng, X. Q. Domestic new energy vehicle sales reached 12.866 million units in 2024. Automobile Review, 2025, (02): 106-107.
- [3] Liu, H. Y. Design and research of a distributed electric vehicle drive controller. Journal of Wuhan Institute of Technology, 2019, 18(4): 86.
- [4] A. K. Yadav, R. M. Pindoriya and B. S. Rajpurohit, "Design and Implementation of Rotor Position Estimation Scheme for PMSM Drive," 2020 IEEE 9th Power India International Conference (PIICON), Sonepat, India, 2020: 1.
- [5] L. Jian, "Research Status and Development Prospect of Electric Vehicles Based on Hub Motor," 2018 China International Conference on Electricity Distribution (CICED), Tianjin, China, 2018: 126

- [6] Guan, T., Liu, D. M., & He, Y. Y. A review of technological development for permanent magnet in-wheel motors. Transactions of China Electrotechnical Society, 2024, 39(2): 379.
- [7] Qiao, J. P. Analysis of the application of in-wheel motor technology in new energy vehicles. Internal Combustion Engine & Parts, 2024, (9): 117-118.
- [8] Chen, G., Yang, Y. Z., Huang, F. H., et al. A review of in-wheel motor development for electric vehicles. Automobile Applied Technology, 2022, 47(4): 142.
- [9] Chen, S., Zhang, X. Y., & Li, P. P. Design of motor control system for in-wheel motor driven electric vehicles. Journal of Shandong Jiaotong University, 2018, 26(2): 10-12.
- [10] Zhang, S. Y. Research on drive control system for in-wheel motors. Huazhong University of Science and Technology, 2019: 48-49.
- [11] Zhao, X. B. A review of motor control technologies for in-wheel drive electric vehicles. Explosion-Proof Electric Machine, 2025, 60(4): 145.
- [12] Wang, Y. Design of a STM32-based FOC controller for brushless DC motors. Information Technology and Informatization, 2010, (8): 145-146.
- [13] SHI Biao, LI Yu Xia, YU Xhua, YAN Wang. Short-term load forecasting based on modified particle swarm optimizer and fuzzy neural network model. Systems Engineering-Theory and Practice, 2010, 30(1): 158-160.
- [14] Amjady N. Short-term hourly load forecasting using time series modeling with peak load estimation capability. IEEE Transactions on Power Systems, 2001, 16(4): 798-805.